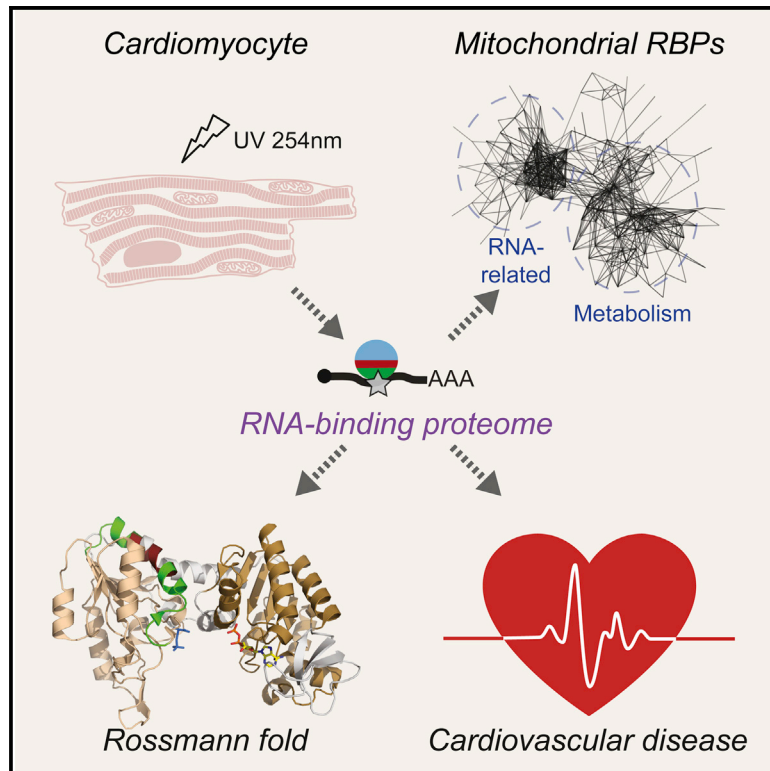# Cell Reports

The Cardiomyocyte RNA-Binding Proteome: Links to Intermediary Metabolism and Heart Disease

Graphical Abstract

Authors

Yalin Liao, Alfredo Castello, Bernd Fischer, ..., Jeroen Krijgsveld, Matthias W. Hentze, Thomas Preiss

Correspondence

thomas.preiss@anu.edu.au

In Brief

RNA functions through dynamic interactions with RNA-binding proteins (RBPs) in all clades of life. In this article, Liao et al. present the RBP repertoire of murine cardiomyocytes. Their findings reflect the unique cardiomyocyte biology and raise the prospect of previously hidden RNA-mediated regulatory interactions between gene expression, physiology, and metabolism.

Highlights

- mRNA interactome capture and RBDmap reveal the cardiomyocyte RNA-binding proteome

- 1,148 RBPs are identified, 393 of which are thus far unique to cardiomyocytes

- Many cardiac RBPs have links to heart disease and mitochondrial metabolism

- Contacts of metabolic enzymes with RNA frequently involve Rossmann fold domains

Accession Numbers

PXD002541
PXD002543

CrossMark

CellPress

The Cardiomyocyte RNA-Binding Proteome: Links to Intermediary Metabolism and Heart Disease

Yalin Liao,[1] Alfredo Castello,[2,4] Bernd Fischer,[2,5] Stefan Leicht,[2] Sophia Föehr,[2] Christian K. Frese,[2] Chikako Ragan,[1] Sebastian Kurscheid,[1] Eloisa Pagler,[1] Hao Yang,[1] Jeroen Krijgsveld,[2,5] Matthias W. Hentze,[2] and Thomas Preiss[1,3,*]

[1]EMBL–Australia Collaborating Group, Department of Genome Sciences, The John Curtin School of Medical Research (JCSMR), The Australian National University, Acton (Canberra) ACT 2601, Australia
[2]European Molecular Biology Laboratory, Meyerhofstrasse 1, 69117 Heidelberg, Germany
[3]Victor Chang Cardiac Research Institute, Darlinghurst (Sydney), NSW 2010, Australia
[4]Present address: Department of Biochemistry, University of Oxford, South Parks Road, Oxford OX1 3QU, UK
[5]Present address: German Cancer Research Centre, 69120 Heidelberg, Germany
*Correspondence: thomas.preiss@anu.edu.au
http://dx.doi.org/10.1016/j.celrep.2016.06.084

SUMMARY

RNA functions through the dynamic formation of complexes with RNA-binding proteins (RBPs) in all clades of life. We determined the RBP repertoire of beating cardiomyocytic HL-1 cells by jointly employing two in vivo proteomic methods, mRNA interactome capture and RBDmap. Together, these yielded 1,148 RBPs, 391 of which are shared with all other available mammalian RBP repertoires, while 393 are thus far unique to cardiomyocytes. RBDmap further identified 568 regions of RNA contact within 368 RBPs. The cardiomyocyte mRNA interactome composition reflects their unique biology. Proteins with roles in cardiovascular physiology or disease, mitochondrial function, and intermediary metabolism are all highly represented. Notably, we identified 73 metabolic enzymes as RBPs. RNA-enzyme contacts frequently involve Rossmann fold domains with examples in evidence of both, mutual exclusivity of, or compatibility between RNA binding and enzymatic function. Our findings raise the prospect of previously hidden RNA-mediated regulatory interactions among cardiomyocyte gene expression, physiology, and metabolism.

INTRODUCTION

RNA-binding proteins (RBPs) are critical interaction partners for all cellular RNAs. RNAs recruit RBPs to form dynamic ribonucleoprotein particles (RNPs), and it is these assemblies that execute RNA function (Castello et al., 2013; Chen and Shyu, 2014; Singh et al., 2015). Multiple sequencing-based RBP footprinting studies (König et al., 2012) have now attested to the long-held view that RBPs interact with RNA in an intricate and highly combinatorial manner (Keene, 2007). The identification of proteins that co-purify with polyadenylated RNA from native cellular contexts by mass spectrometry, dubbed mRNA interactome capture, has yielded the first comprehensive views of active RBPs in eukaryotic cells. Specifically, mRNA interactome capture from human cervical cancer (HeLa) (Castello et al., 2012) and embryonic kidney (HEK293) cells (Baltz et al., 2012), murine embryonic stem cells (ESCs) (Kwon et al., 2013), S. cerevisiae (Beckmann et al., 2015; Matia-González et al., 2015; Mitchell et al., 2013), C. elegans (Matia-González et al., 2015), as well as human hepatoma cells (HuH-7) (Beckmann et al., 2015) together identified over 1,000 RBPs, many of which had no prior RNA-related annotation. Despite this already considerable expansion of mRNP componentry, more distinct cellular contexts need to be studied to define context-specific RBP repertoires.

The identification of so many RBPs indicates hitherto-unknown connections between seemingly disparate cellular processes and unexpected "moonlighting" activities that proteins carry out in a highly compartmentalized cellular environment (Copley, 2012). One such area deserving of further exploration is suggested by the reported ability of several metabolic enzymes to interact with RNA (Castello et al., 2015; Cieśla, 2006; Hentze, 1994; Hentze and Preiss, 2010). Enzymes could moonlight to regulate mRNA utilization in response to co-factor or metabolite levels, as documented for the cytosolic aconitase (ACO1)/iron regulatory protein (IRP1) paradigm (Muckenthaler et al., 2008). Conversely, RNA could affect enzyme activity, and collectively these interactions could form regulatory RNA-enzyme-metabolite (REM) networks (Hentze and Preiss, 2010).

Here, we report the adaptation and parallel application of mRNA interactome capture (Castello et al., 2012) and RBDmap (Castello et al., 2016) to beating murine HL-1 cardiomyocytes (Claycomb et al., 1998). We chose cardiomyocytes because of their unique metabolic requirements and importance to human disease (Rosca et al., 2013), gaining insight especially into the scope of mitochondrial RBPs.

RESULTS

mRNA Interactome Capture and RBDmap Uncover the RNA-Binding Proteome of Cardiomyocytes

Both proteomic methods require large numbers of cells, and thus we employed the murine HL-1 cardiomyocyte cell line as readily renewable source material. HL-1 cells are widely used
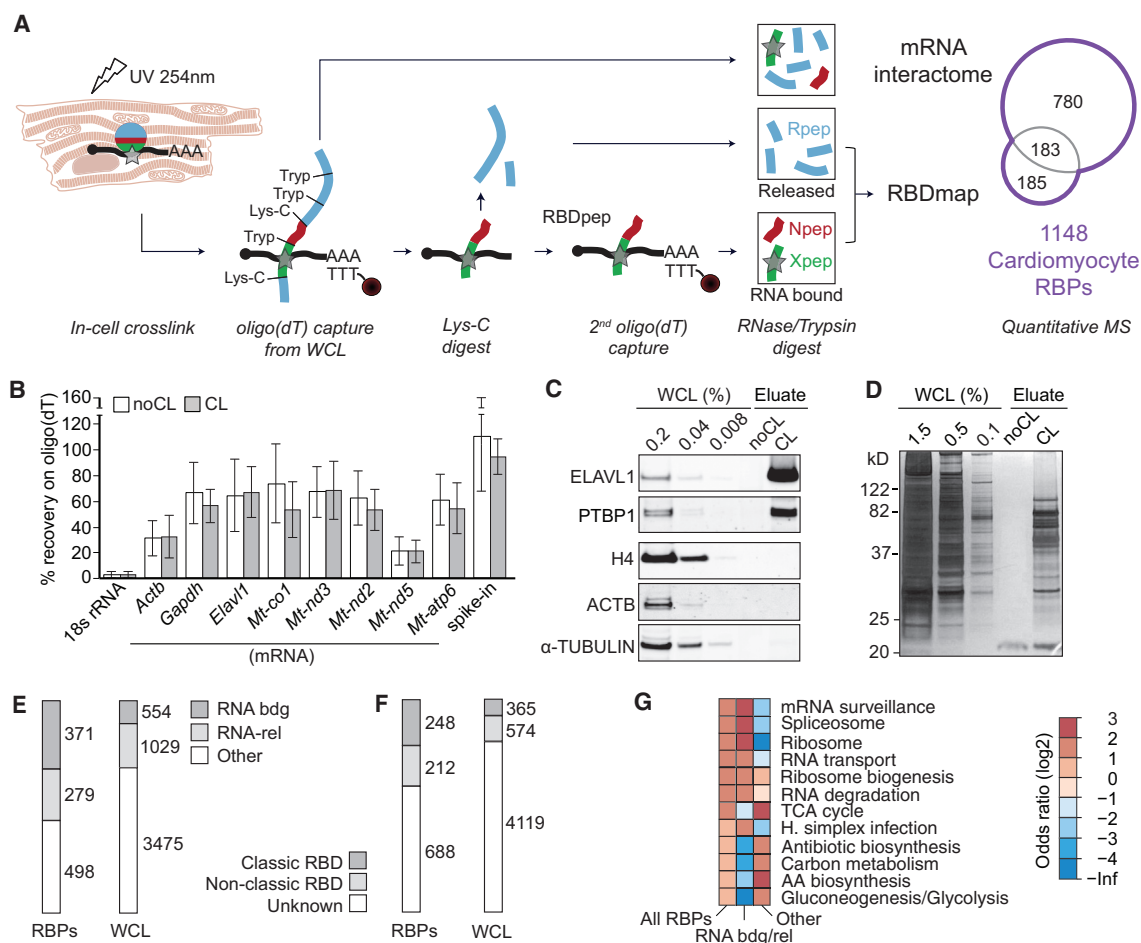
Figure 1. Identification of Cardiomyocyte RBPs

(A) Schematic of mRNA interactome capture and RBDmap approaches. Proteins identified by one or both approaches constituted a superset of cardiomyocyte RBPs.

(B) RNA-protein complexes captured on oligo(dT) beads were digested with proteinase K and RNA recovery levels monitored by quantitative PCR. Shown are averages of six biological replicates. Error bars, SD.

(C and D) Complexes captured on oligo(dT) beads were eluted by RNase-digestion, resolved by SDS-PAGE alongside input WCL (percentage equivalent to loaded eluate amount as indicated), and analyzed by western blot (C; see Experimental Procedures for antibody details) or silver stain (D). Results are representative of three independent interactome capture experiments. (See Figures S1A and S1B for equivalent RBDmap controls.)

(E) Proportion of cardiomyocyte RBPs or WCL proteins with GO annotation "RNA binding" or RNA-related annotations (see Supplemental Experimental Procedures for details on annotation sources). Left, cardiomyocyte RBPs; right, WCL.

(F) Analyses as in (E) for RBDs.

(G) Matrix plot of enriched/depleted KEGG pathways among RBP groups as defined in (E), compared to WCL.

See also Figures S1 and S2 and Table S1.

as a model as they retain many characteristics of adult cardio-myocytes (Claycomb et al., 1998), although compared to native myocardium their energy metabolism is less organized (e.g., Eimre et al., 2008). Confluent and spontaneously beating murine HL-1 cells were irradiated with UV light (150 mJ/cm^2 at 254 nm) to induce covalent crosslinks (CLs) between proteins and RNA within native complexes. Under these conditions, crosslink formation will typically be sub-stoichiometric and selectively occur at "zero" distance protein-RNA interactions (Castello et al., 2012, 2016). After denaturing cell lysis, RNA-protein complexes were captured on oligo(dT) beads and washed with high-salt/anionic detergent buffer to remove non-crosslinked proteins.

Bound material was then processed for "mRNA interactome capture" to determine the scope of cardiomyocyte RBPs or for "RBDmap", which maps protein regions contacting RNA, as schematized in Figure 1A. Three independent biological replicates were processed for each approach, as well as parallel non-crosslinked controls (noCL). Aliquots taken after the first round of capture demonstrated selective purification of polyadenylated RNAs (cytosolic and mitochondrial; Figure 1B), known RBPs such as ELAVL1 and PTBP1 (Figures 1C and S1A), and a distinct subset of cellular proteins as the mRNA interactome (Figures 1D and S1B). For mRNA interactome capture (Castello et al., 2012), RBPs were liberated by RNase treatment, digested

with Trypsin/Lys-C protease mix, and analyzed by quantitative mass spectrometry. This identified 963 high-confidence RBPs (false discovery rate [FDR], 1%; see Figure S1D for reproducibility between replicates). Mass spectrometry was also performed on whole-cell lysate (WCL) samples, which identified 4,749 proteins (Table S1).

The RBDmap approach is described and validated in detail elsewhere (Castello et al., 2016). In applying RBDmap here, complexes eluted after a first round of capture were digested with Lys-C only, before a second round of oligo(dT) purification (Figure S1C). This separated protein fragments into a "released" and an "RNA bound" pool, which were both treated with RNase and Trypsin. All tryptic fragments within the released pool, termed Rpeps, can in principle be detected by mass spectrometry (Figure 1A). By contrast, tryptic digestion of the "RNA-bound" pool will yield two types of peptides. One type (termed Xpep, depicted in green, Figure 1A) will still carry a remnant, or remnants, of crosslinked RNA. Due to this heterogeneous mass shift, Xpeps are difficult to be detected by mass spectrometry (see Castello et al., 2016; Kramer et al., 2014). The other type (termed neighboring peptide or Npep, depicted in red, Figure 1A) is of predictable mass and thus readily detectable. Extension from the Npep boundaries to adjacent Lys-C sites can nevertheless still predict the Xpep coordinates, although sub-stoichiometric crosslinking and protease cleavage will add some complexity to the assessment of individual examples. Note that proteolytic processing efficiency is close to 100% (Figure S1C). Therefore, matching Npep and Xpep(s) together constitute the original RNA-bound Lys-C fragment (termed RBDpep, Figure 1A). Proteins derived from 368 genes exhibited RBDpeps that were enriched in the RNA bound over the released pool at an FDR of 1% (see Figure S1E for reproducibility between replicates).

Proteins that lack a Trypsin cleavage site within their RBDpeps will not be "visible" by RBDmap but may still be detected by mRNA interactome capture. Conversely, the additional proteolytic step and enrichment by a second oligo(dT) capture round in RBDmap will reduce sample complexity and experimental noise, thus improving detection for another subset of proteins (Castello et al., 2016). Consequently, proteins identified by RBDmap substantially (65%), but not completely, overlap with those of the mRNA interactome approach (183 RBPs are shared with the HL-1 mRNA interactome Figure 1A; an additional 51 are shared with the following mRNA interactomes: HeLa, HEK293, HuH-7). Taken together, both approaches define a "superset" of 1,148 cardiomyocyte RBPs (Tables S1, S2, and S3).

Known and Uncharacterized Cardiomyocyte RBPs Share Similar Functional Features

Compared to the WCL proteome, cardiomyocyte RBPs were enriched for RNA-related functions (56% have RNA-related annotation, Figure 1E; see Figure S1F for the most enriched/depleted Gene Ontology [GO] terms), as expected. A similar GO term enrichment was seen with either the mRNA interactome or RBDmap set individually (data not shown). KEGG pathway enrichment analysis confirms this but interestingly also indicates overrepresentation of several pathways of intermediary metabolism among RBPs without prior RNA-related annotation (Figure 1G; see below). Similarly, proteins with classic or non-classic RNA-binding domains (RBD) are also overrepresented (Figure 1F). Many known RBD types are enriched among the cardiomyocyte RBPs (Figures S1G and S1H). For instance, we captured most of the RRM-containing proteins expressed in HL-1 cells (139 out of 168; Figure S1G). Similar trends were seen for other RBDs, including DEAD box helicase, KH, PWI, and PUF domains as well as many of the expected zinc finger domain subtypes (Figures S1I and S1J). We further identified all eight proteins with the MIF4G fold expressed in HL-1 cells as RBPs (i.e., EIF4G1-3, UPF2, CWC22, CTIF, NOM1, NCBP1). These proteins relate to the nexus of mRNA splicing, translation initiation, and nonsense-mediated decay. Enrichment of the Nol1_Nop2_Fmu domain was driven by capture of four members of the NSUN family of RNA:m^{5}C (5-methylcytosine) methyltransferases (NSUN1, -2, -4, -5). Nucleoside modifications in polyadenylated RNA have received much attention lately and indeed, 29 proteins with annotations related to "RNA modification" were detected as cardiomyocyte RBPs (Table S3), prominently covering the enzymology of m^{5}C, m^{6}A (N^6-methyladenosine), and pseudouridine modifications, as well as adenosine to inosine editing, all shown to occur in mRNA (Jaffrey, 2014; Sibbritt et al., 2013). Beyond that, we find componentry involved in several additional RNA modifications, including m^{5}U (5-methyluridine), m$^6_2$A (N^6,N^6-dimethyladenosine), and D (dihydrouridine), suggesting that the diversity of RNA modifications in polyadenylated RNAs may be richer than currently documented. All seven mammalian pentatricopeptide repeat (PPR)-containing proteins were identified here. PPR proteins function in mitochondrial RNA metabolism (Lightowlers and Chrzanowska-Lightowlers, 2013) and recognize RNA in a modular manner (Filipovska and Rackham, 2013). Several other protein domains lacking reported RNA-binding activity were also well represented in our datasets (Figure S1K), possibly reflecting direct involvement in RNA binding in some cases. Histones were notable (mostly H1 and H2A variants), possibly relating to the known association of RNA with chromatin (Mondal et al., 2010). Consistent with observations in the HeLa cell mRNA interactome (Castello et al., 2012), we detected RNA binding by 11 peptidyl-prolyl isomerases (PPIases, Table S3). Several of these are known for their involvement in nuclear gene expression (i.e., chromatin structure, gene transcription, mRNA splicing, and export) and some have recognized RBDs (Schiene-Fischer, 2015); however, for others these findings suggest hitherto-unknown roles for RNA in PPIase biology and pathology (see below).

Cardiomyocyte RBPs also display the biophysical and sequence features expected of bona fide RBPs. They range from low to high abundance, with some tendency toward higher abundance compared to the WCL proteome (Figure S2A), reflecting similar observations reported elsewhere (Castello et al., 2016; Matia-González et al., 2015). Cardiomyocyte RBPs have no length bias, but they are shifted toward a more alkaline isoelectric point and lower hydrophobicity (Figures S2B–S2D), as reported for other mRNA interactomes (Castello et al., 2012; Kwon et al., 2013). They further display an elevated content of intrinsically disordered regions and are enriched for the amino acids arginine (R), lysine (K), tyrosine (Y), and glycine (G)
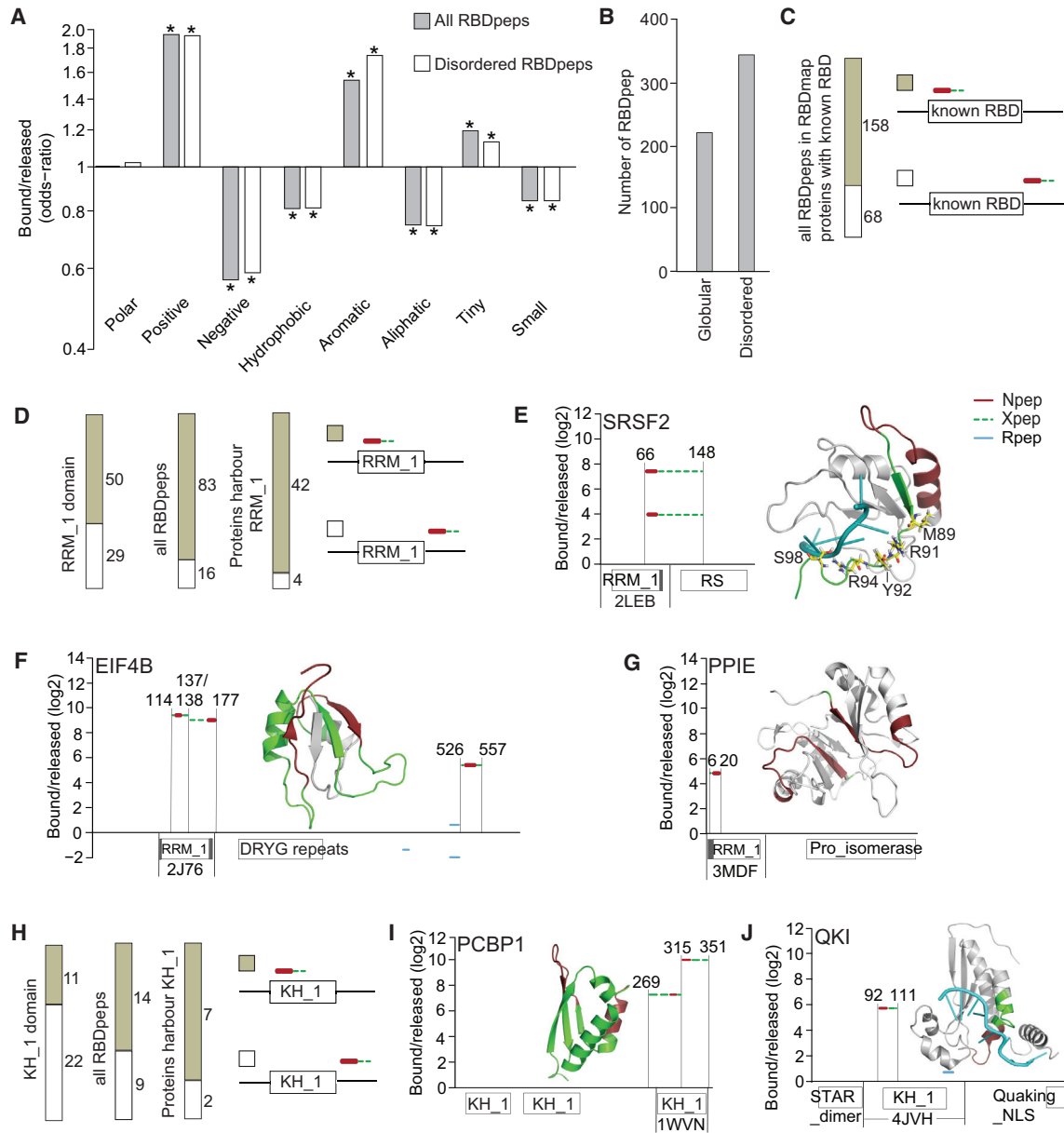
Figure 2. Performance of the RBDmap Approach

(A) Analysis of amino acid bias in RBDpeps (cf. Figure 1A) and disordered RBDpeps versus corresponding released fragments. *p < 0.01.

(B) RBDpep distribution between globular and disordered protein domains.

(C) Proportion of RBDpeps that overlap with a known RBD.

(D) In RBDmap proteins containing RRM_1, proportion of RRM_1 motifs with RBDpep coverage (left), of RBDpeps that overlap with an RRM_1 (middle) and of RRM_1-containing RBPs with at least one such overlap (right).

(E) Graphic representation of RBDmap data for SRSF2. Here, as in subsequent panels/figures displaying RBDmap data, Npeps (red) and Xpeps (green dashes; the crosslinked amino acid could reside anywhere within the Xpep), jointly termed RBDpep (positions of N- and C- termini are indicated), are mapped onto the linear protein sequence. y axis indicates enrichment (log2) in RNA bound over released fraction. Boxes underneath the x axis indicate Pfam-annotated domains with extensions (shaded gray) based on crystal structures, unless otherwise specified. See Supplemental Experimental Procedures for RS domain annotation. RBDpeps were also highlighted in the co-crystal structure (PDB: 2LEB) of the SRSF2 RRM_1 domain (ribbon diagram) with 5′-UCCAGU-3′ RNA (teal). Amino acids contacting RNA in structure are rendered as stick models.

(F) RBDmap data for EIF4B and crystal structure of the EIF4B RRM_1 (PDB: 2J76). Rpeps are shown in blue. DRYG repeats position was obtained from Méthot et al. (1996).

(G) RBDmap data for PPIE and crystal structure of PPIE RRM_1 dimer (PDB: 3MDF).

(legend continued on next page)

(Figures S2E and S2F). Low-complexity and repetitive regions, known to favor formation of RNA-protein granules (Kato et al., 2012) and to frequently occur in RBPs (Castello et al., 2012), are also overrepresented (Figures S2G and S2H). All of these features also apply to the subset of 688 cardiomyocyte RBPs lacking previously known RBDs. Amino acid patterns that center around the enriched residues R, K, Y, S, and G include RS repeats often found in splicing factors and resemble RGG and YGG boxes or poly(K) stretches, each previously implicated in RNA binding (Figure S2I) (Castello et al., 2012).

Overall, the RNA-binding proteome of cardiomyocytes shows substantial overlap with other mRNA interactomes: 429 RBPs are shared with the murine ESC set (Kwon et al., 2013), and 717 are in common with three available human mRNA interactomes from HEK293, HeLa, and HuH-7 cells (Baltz et al., 2012; Beckmann et al., 2015; Castello et al., 2012). 391 "core" RBPs emerge as "in common" between all reported mammalian mRNA interactomes, while 393 RBPs are thus far unique to the cardiomyocyte RBP set (Figure S2J). As expected, the core RBPs are particularly enriched for RNA-related GOMF annotations and recognized RBDs. The "unique" cardiomyocyte RBPs have lower proportions of these attributes and instead feature elevated proportions of proteins with mitochondrial localization, links to cardiovascular disease and development, genetic disease, and metabolic enzyme function (Figure S2K). This likely reflects the unique physiology of cardiomyocytes, e.g., their heavy reliance on mitochondrial metabolism, and their importance to human disease, aspects that we explore further below.

Benchmarking Cardiomyocytic RBD Assignments by RBDmap

RBDmap identified 568 RBDpeps at 1% FDR, representing RNA-binding regions of 368 cardiomyocyte RBPs. The distances between Lys-C and Trypsin cleavage sites in individual proteins define the resolution achievable by RBDmap by determining the lengths of individual RBDpeps, Npeps and Xpeps (range/median: 7–161/20 amino acids (aa) for RBDpeps, 7–30/11 aa for Npeps, 1–148/11 aa for Xpeps) (Figure S3A). Limitations of RBDmap are that some protein-RNA contacts can be absent from the data due to (1) absence of suitable crosslink geometry; (2) lack of trypsin cleavage site(s) within RBDpeps; and (3) peptide detection biases of mass spectrometry. Moreover, Xpep can only give the boundaries within which the actual RNA-protein crosslink site is situated but cannot locate it further (see Castello et al., 2016 for a comprehensive evaluation). That said, RBDpeps and released peptides exhibit the expected divergent properties. Positively charged (R, K), aromatic (F, W, Y, H), and tiny amino acids (A, G, S, T, C) are enriched among RBDpeps, whereas negatively charged (D, E) and aliphatic amino acids (I, L, V) are more prevalent in released peptides (Figure 2A). A majority (347, 61.1%) of RBDpeps map to disordered regions (Figure 2B), and this subset retains the same amino acid bias (Figure 2A),

evoking a broader role of disordered regions in RNA binding. These observations match those with RBDmap of HeLa cells (Castello et al., 2016).

To assess the consistency of RBDmap assignments, we identified proteins with homologs present in both the HL-1 and HeLa datasets (Figure S3A) and tested for concordance of RNA-binding site identifications. Approximately two-thirds of the associated mouse RBDpeps (161 of 237) had an equivalent counterpart in the human dataset (Figure S3B), a high proportion given the use of different cell lines from different organisms as well as the relative inefficiency and spatial limitations of UV crosslinking (Castello et al., 2012). Next, we examined the RBDmap data of 116 proteins with a classic or non-classic RBD. 158 of 226 RBDpeps derived from these proteins mapped to one of the known RBDs (Figure 2C). Forty-six of these proteins contained a total of 79 RRM_1 motifs. Reassuringly, RBDpeps overlapped with 50 of these RRM_1 motifs, and RNA binding mapped to at least one of their RRM_1 motifs for 42 out of the 46 protein examples examined (Figure 2D). Ten of the 12 members of the serine/arginine-rich splicing factor (SRSF) family (Busch and Hertel, 2012) were identified as cardiomyocyte RBPs (Figure S3C); seven of these have coverage in RBDmap. In each case, the RBDpep clearly overlaps with the first RRM_1 motif (Figures 2E and S3D–S3I). For SRSF2, the Xpep interval spans the C-terminal part of RRM_1 and extends into the RS domain. RS domains were proposed to bind RNA as well (Shen and Green, 2006). However, as there is prior evidence that RNA binding to SRSF2 does not require the RS domain (Daubner et al., 2012), the RNA crosslink(s) likely occurred within the C-terminal region of the RRM_1 domain. This would nicely reflect the crystal structure of the RRM_1 domain of SRSF2, which features direct RNA contacts within this region (Figure 2E, right panel). EIF4B and the splicing-associated PPIase PPIE are other proteins confirmed by RBDmap to contact RNA through their RRM_1 domain (Figures 2F and 2G). Nine KH domain proteins, containing a total of 33 KH motifs, were also part of the RBDmap dataset. Here, RBDpeps overlapped with 11 KH motifs, and RNA binding mapped to at least one of their KH motifs for seven out of the nine proteins examined (Figure 2H). Examples are the translational regulator poly(rC) binding protein 1 (PCBP1) (Ostareck et al., 1997) (Figure 2I) and the splicing regulator quaking (QKI) (Hall et al., 2013) (Figure 2J). Of further interest, RBDmap also marked a region adjacent to the NHL repeat domains in the E3 ubiquitin ligase TRIM2, consistent with recent reports that TRIM-NHL proteins are sequence-specific RNA-binding proteins (Kwon et al., 2013; Loedige et al., 2015), and the multiple zinc finger domains of the nuclear pore component and PPIase RANBP2, known to bind mRNAs encoding secretory proteins to promote their translation (Mahadevan et al., 2013) (data not shown). Taken together, these findings support the ability of RBDmap to identify protein regions in contact with RNA.

(H) Analyses as in (D) but for KH_1 motifs.
(I) RBDmap data for PCBP1 and crystal structure of the third KH_1 motif of PCBP1 (PDB: 1WVN).
(J) RBDmap data for QKI and crystal structure of QKI KH_1 in complex with 5′-ACUAACAA-3′ RNA (teal) (PDB: 4JVH).
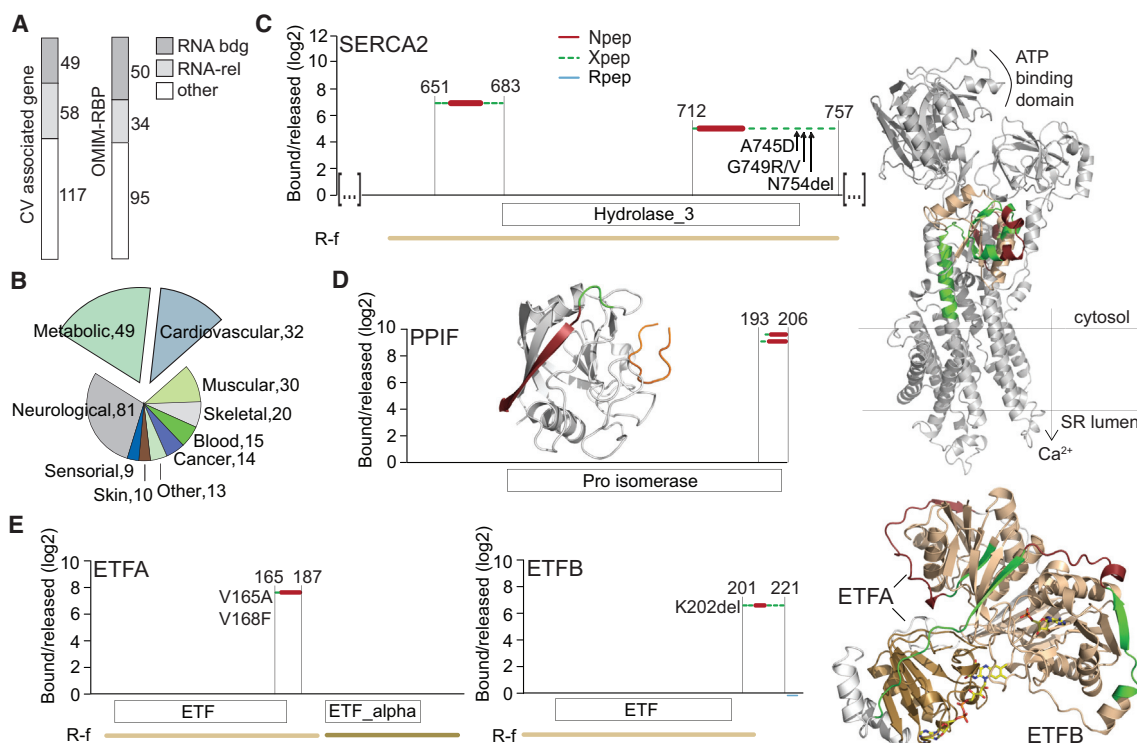See also Figure S3 and Table S2.

Figure 3. Association of Cardiomyocyte RBPs with Cardiovascular Disease/Development and Human Mendelian Diseases
(A) Analyses as in Figure 1E but for RBP association with cardiovascular disease/development (left) and genetic disease (based on OMIM; right).
(B) Spectrum of OMIM-listed genetic diseases caused by mutations in cardiomyocyte RBPs.
(C) RBDmap data for SERCA2 (amino acids 612–758; EC:3.6.3.8) and mapping onto Phyre2-modeled structure. Arrow indicates position of disease-associated missense mutation variants. A R-f domain is also highlighted (wheat).
(D) RBDmap data for PPIF (EC:5.2.1.8) and mapping onto co-crystal structure (PDB: 4TOT) of PPIF with inhibitor NIM258 (orange, PDB: 4TOT).
(E) RBDmap data for ETFA/ETFB and mapping onto crystal structure in complex with FAD and AMP (multicolor; 1EFV). A second R-f domain in ETFA is highlighted with a sand color.
See also Tables S3 and S4.

Cardiomyocyte RBPs Have Rich Links to Heart Biology and Genetic Disease

Next, we defined human orthologs to murine cardiomyocyte RBPs to investigate links with heart function and disease. 222 cardiomyocyte RBPs relate to cardiovascular disease and development, based on the Cardiovascular Gene Ontology Annotation Initiative, and 117 of these had no prior RNA-related annotation (Figure 3A, left; Table S3). Similarly, 179 cardiomyocyte RBPs, when mutated, are known to cause genetic disease based on the Online Mendelian Inheritance in Man (OMIM) database; 84 of these have prior RNA-related annotation, while 95 lack it (Figure 3A, right; Table S3). A notable example of the former is the RRM_1/SR domain-containing splicing factor RBM20, known to cause dilated cardiomyopathy when mutated (Brauch et al., 2009) RBM20 is primarily expressed in striated muscle, with the highest levels found in the heart (Guo et al., 2012). Consistently, among the available mammalian mRNA interactomes it was uniquely detected in the HL-1 cardiomyocytes. Collectively, the OMIM-RBPs are associated with a spectrum of 273 genetic diseases (Table S4). We find neurological, metabolic, and cardiovascular disorders as the most prominent types of disease (Figure 3B). Together, these account for 59% of

the diseases, highlighting the potential relevance of RNA binding to a molecular understanding of multiple genetic disorders and reflecting the common co-occurrence of neurological and cardiac manifestations of disease due to their high energy requirements (see below).

RBDmap data were available for 71 of the OMIM-RBPs (35 without prior RNA-related annotation) and for 12 of these RBDpeps cover known missense mutations or amino acid deletions (Table S3). Examples are HNRNPA2B1 and TARDBP, RRM-containing proteins that also harbor low-complexity regions or prion-like domains (PrLDs) with roles in RNA granule formation. Mutations in the PrLD of RBPs are implicated in neurodegenerative diseases, e.g., in HNRNPA2B1 and TARDBP, they cause multisystem proteinopathy and amyotrophic lateral sclerosis, respectively (Kim et al., 2013; King et al., 2012). Separate RBDpeps cover not only the RRM domain, but also the PrLD, overlapping with known disease mutations for both proteins (data not shown), raising the prospect of defective RNA binding as an additional disease mechanism in affected tissues. Seven of the 12 OMIM-RBPs lack prior RNA-related annotation and are of particular interest. For example, sarcoplasmic/endoplasmic reticulum calcium ATPase 2 (SERCA2)

has cardiovascular relevance as well as links to genetic disease. It regulates heart muscle contractile function by sequestration of calcium to the lumen of the sarcoplasmic reticulum during relaxation. SERCA2 activity is decreased during heart failure, and gene therapy trials to restore its function have shown promise (Gorski et al., 2015). Mutations in SERCA2 further cause the skin disorder Darier's disease (Zheng et al., 2015). RBDmap data locate the RNA-binding activity of this protein to a region adjacent to the ATP binding site in the cytosolic domain (Figure 3C). Interestingly the RBDpep overlaps with four known Darier's disease mutations (G749R, A745D, N754del [annotated in OMIM], G749V [Zheng et al., 2015]), suggesting a possible pathogenic role of altered RNA binding. Ten members of the aforementioned PPIase family have been implicated in cardiovascular disease (Perrucci et al., 2015). We identified four of these as RBPs: PPIC, -D, -F, and FKBP1A, the latter three also have RBDmap data (Table S3). PPIF regulates the mitochondrial permeability transition pore to affect mitochondrial calcium homeostasis and is involved in multiple cardiovascular pathologies (Perrucci et al., 2015). RBDmap locates RNA binding to the pro-isomerase domain of PPIF, in close proximity to a pharmacological inhibitor-binding site (Figure 3D).

Electron transfer flavoprotein (ETF) is a heterodimer located in the mitochondrial matrix and functions in the transfer of electrons from fatty acid oxidation (FAO), amino acid, and choline catabolism to oxidative phosphorylation (OXPHOS). The complex binds FAD in a cleft formed by the C-terminal domain of the α subunit (ETFA), and the β subunit (ETFB); AMP is bound entirely within ETFB. Mutations in ETF lead to the metabolic disorder multiple acyl-CoA dehydrogenase deficiency (MADD or GA-II) (Schiff et al., 2006). RBDmap detects RNA binding to both subunits, with RBDpeps mainly residing on the exterior of the complex, away from the FAD and AMP sites (Figure 3E). The RBDpeps overlap with three known MADD mutations (ETFA: V165A, V168F; ETFB: K202del [annotated in OMIM]). The occurrence of disease-causing mutations within regions of RNA contact thus suggests a role of RNA in a number of disease pathologies.

Domains of the Rossmann Fold Topology Commonly Bind RNA

The enrichment of annotation relating to intermediary metabolism (Figure 1G) is driven by the presence of 73 metabolic enzymes (for a definition, see Supplemental Experimental Procedures) among the cardiomyocyte RBPs, densely covering cytosolic glycolysis as well as mitochondrial FAO, the TCA cycle, and OXPHOS (see below). Among these RNA-binding enzymes (Table S5; 24 with RBDmap data) are ten examples with prior "classic" literature (Castello et al., 2015; Cieśla, 2006; Copley, 2012; Hentze, 1994; Hentze and Preiss, 2010); another 13 were identified as RBPs by previous mRNA interactome studies, which identified a total of 23 metabolic enzymes (Baltz et al., 2012; Castello et al., 2012; Kwon et al., 2013). Enzyme Commission (EC) classification EC1 (oxidoreductases; 33 examples) and EC2 (transferases; 25 examples) are particularly prevalent among the set of 73 RNA-binding enzymes (Figure 4A). Notably, most of these interact with either mono or di-nucleotides, e.g., ATP/GTP or NAD(P)$^+$/FAD, a function often carried out by a glob-

ular domain referred to as Rossmann fold (R-f). This domain is characterized by a six-stranded parallel β sheet with interlinking α helices on either side of the sheet (Caetano-Anollés et al., 2007; Rossmann et al., 1974). Thus, we used CATH/Gene3D annotation (Sillitoe et al., 2015) to search for R-f topology (CATH id: 3.40.50). 692 proteins in WCL match this topology, and, while there was no significant enrichment of R-f proteins among cardiomyocyte RBPs, it was still striking that 173 of them harbored a R-f domain. Among the R-f RBPs, 87 are with and 86 are without prior RNA-related annotation (Figure 4B; Table S3). 43 of R-f RBPs are covered by RBDmap data, and 33 of 61 RBDpeps derived from these proteins mapped to a R-f domain (Figure 4C). The group of R-f RBPs without prior RNA-related annotation is rich in metabolic enzymes but also includes other functions such as the aforementioned Ca^{2+} ATPase SERCA2 (Figure 3C) and the flavoproteins ETFA&B (Figure 3E). Among the R-f superfamilies 3.40.50.300 ("P loop containing nucleotide triphosphate hydrolases"; 96 examples) is the most prevalent (Figure 4D). It includes 42 RNA helicases (27 DEAD-box, eight DEAH/RHA, three UPF1-, one Ski2-like, and three others) representing one-half of the 87 R-f RBPs with prior RNA-related annotation (Figures 4B and 4E). Notably, other members of the superfamily 3.40.50.300 include several DNA helicases. The large number of cardiomyocyte RBPs classified within the superfamily 3.40.50.720 ("NAD(P)-binding Rossmann-like Domain"; 18 examples) reflects the prevalence of metabolic enzymes among the RBPs lacking prior RNA-related annotation: 13 of the EC1 enzymes among the RBPs display the 3.40.50.720 R-f topology. Other well-represented superfamilies are 3.40.50.150 ("Vaccinia Virus protein VP39"; 18 examples), which references the presence of RNA-modifying enzymes, and 3.40.50.620 (HUPs; nine examples), common among tRNA synthetases. Taken together, the R-f topology emerges prominently among RBPs, both with and without prior RNA-related annotation.

The structural core of superfamily 1 and 2 helicases is composed of two helicase domains, each with R-f topology. ATP binds in a cleft formed by the two domains, while the nucleic acid contacts with the R-f domains are on the opposite surface of this core (Fairman-Williams et al., 2010), as exemplified by the co-crystal structure of EIF4A3 with RNA (Figure S4A). RBDmap data locate RNA-binding sites within nine helicases (DDX5, -17, -21, -27, -46; DHX8, -15, UPF1 and ASCC3). Structural modeling shows that the RBDpep overlaps with the expected RNA contact surface for the pre-mRNA splicing factor DHX15 (Figure 4F) and three additional examples (Figures S4B, S4C, and S4I). Interestingly, ASCC3 was previously described as a DNA helicase (Dango et al., 2011), while it is identified as an RBP here (Figure S4I). For DDX17, DDX27, DDX5, DHX8, and UPF1 the RBDpeps map to N-or C-terminal extensions of the helicase (Figures S4D–S4H), indicating additional RNA contacts beyond the helicase core. In UPF1, for example, the RBDpep maps to the C-terminal SQ domain that physically interacts with the central core and inhibits helicase activity (Figure S4H) (Fiorini et al., 2013). Notwithstanding these latter observations, our RBDmap data broadly concur with the expected arrangement of RNA contact sites within helicase R-f topology domains.

29 of the 73 metabolic enzymes identified here as RBPs have at least one annotated R-f. Inspection of available crystal
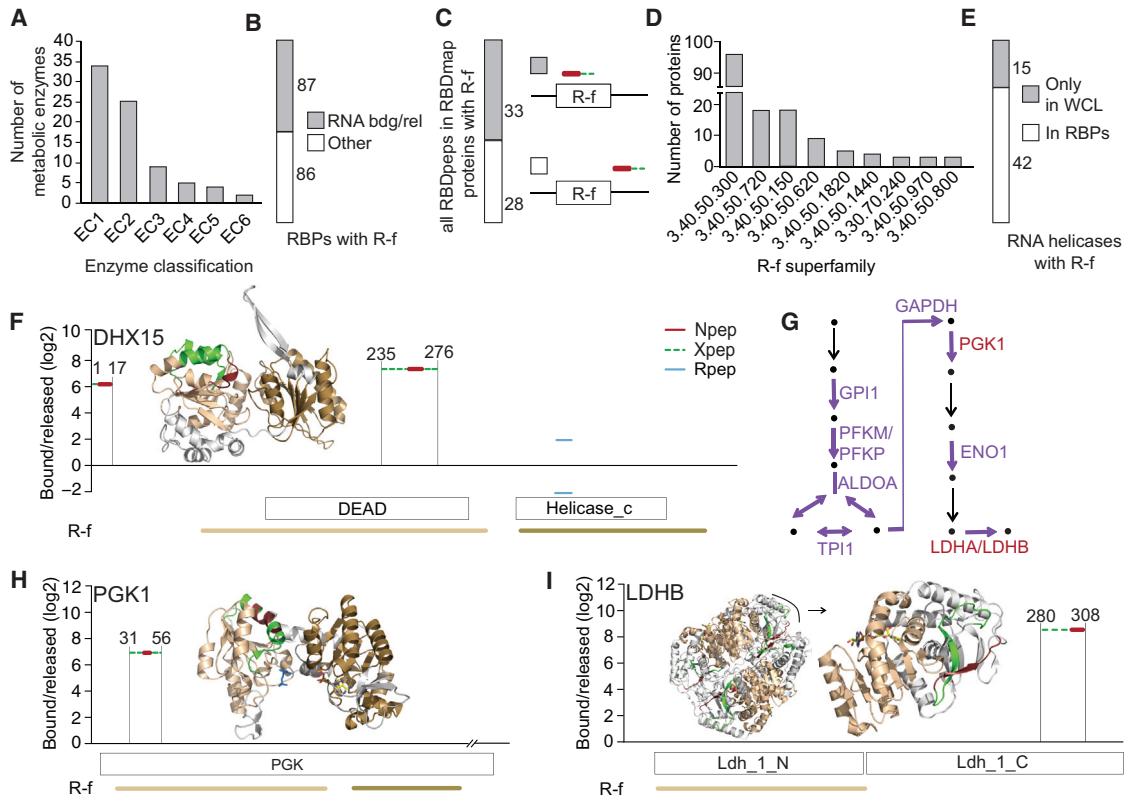
Figure 4. Rossmann Fold Topology and RNA Binding

(A) Classification of metabolic enzymes among cardiomyocyte RBPs.

(B) Analysis as in Figure 1E for R-f cardiomyocyte RBPs.

(C) Proportion of RBDpeps that overlap with a R-f domain.

(D) Distribution of cardiomyocyte RBPs across R-f superfamilies (by CATH id; only families with more than three members are shown).

(E) Proportion of WCL RNA helicases with R-f identified as RBPs.

(F) RBDmap data for DHX15 and mapping onto Phyre2-modeled structure. Here, and in the following panels, R-f domains are highlighted as applicable (N-terminal, wheat; C-terminal, sand).

(G) Schematic of glycolysis. Purple and red color indicate enzyme(s) present in cardiomyocyte RBPs and the RBDmap dataset, respectively.

(H) RBDmap data for PGK1 (EC:2.7.2.3) and mapping to tetrameric crystal structure in complex with 3-phosphoglyceric acid (orange) and ADP (multicolor) (PDB: 2XE7).

(I) RBDmap data for LDHB (EC:1.1.1.27) and mapping to tetramer crystal structure in complex with NAD$^+$ (multicolor) (PDB: 1I0Z). Enlarged view shows monomer.
See also Figures S4, S6, and S7 and Tables S3 and S5.

structures identified further enzymes that have domains of similar topology, increasing this list to 41 entries (Table S5). 27 of these bind either mono- (nine) or di-nucleotides (19). Available RBDmap data for 16 examples (25 RBDpeps) shows overlap between RNA binding and the R-f in 12 cases, including PGK1 from the densely covered glycolysis pathway (Figures 4G and 4H; further examples are shown in Figures 7, S6, and S7). In four additional cases the RBDpeps are spatially close to the R-f, including another glycolysis enzyme, LDHB (Figures 4I). This shows that the involvement of R-f topology domains is common among metabolic enzymes that bind RNA, confirming long-held expectations (Hentze, 1994). Unlike the helicases, R-f topology as well as tertiary and quaternary structure is more diverse among the metabolic enzymes, and thus we found the arrangement of RNA binding relative to R-f domain orientation also to be more varied.

In-Depth Characterization of the Mitochondrial mRNA Interactome

Cardiomyocytes belong to the most highly energy-consuming cell types and are rich in mitochondria. 18.0% of WCL proteins are annotated with the GO term "mitochondrion," and this proportion is similar among cardiomyocyte RBPs (16.3% or 187 proteins; Figure S5A; 49 with RBDmap data). RNA and RBD-related annotations are highly represented among these mitochondrial mtRBPs (Figures S5B and S5C). Protein network analysis reveals two major groupings among mtRBPs: the first represents RBPs with known roles in RNA biology, while the second is centered on intermediary metabolism (Figure 5A). Among the 88 mtRBPs with known RNA roles (17 had RBDmap data), we found that all steps in the mitochondrial RNA life cycle (Rackham et al., 2012) are richly represented (Figure 5B). Cross-referencing the proteome of mitochondrial RNA processing granules
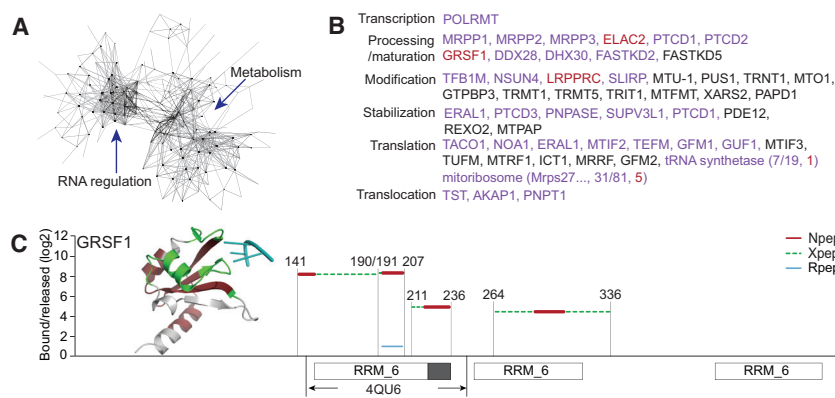
(Antonicka and Shoubridge, 2015), we further noticed an overlap with 54 of our mtRBPs. These include six PPR proteins, ranging from the mitochondrial RNA polymerase POLRMT, through the polycistronic pre-RNA processing factors LRPPRC, MRPP3 and PTCD1, to the translation regulators PTCD3 and MRPS27. All three subunits of the mitochondrial RNase P complex belong to this cross-section, as well as three recently described RNA granule components, FASTKD2, DDX28, and DHX30 (Antonicka and Shoubridge, 2015). RBDmap demarcates RNA binding to the first two RRM_6 domains of GRSF1 (Figure 5C), a central mitochondrial RNA granule component (Jourdain et al., 2013).

The 99 mtRBPs without prior RNA-related annotation (32 with RBDmap data) are dominated by 49 metabolic enzymes, densely covering FAO, TCA cycle, and OXPHOS (Figure 6A). Interestingly, the mitochondrial RNA granule proteome of 143B cells similarly contains multiple mitochondrial metabolic enzymes (Antonicka and Shoubridge, 2015); nine of these are shared with the list reported here. Is this an indication of a widespread role of RNA binding by mitochondrial metabolic enzymes? Of note, the MRPP3 subunit of RNase P has a PPR RBD, MRPP1 moonlights as an m^{1}G$_9$ RNA modifying enzyme and HSD17B10/MRPP2, is also an NAD$^+$-dependent short-chain fatty acid dehydrogenase (Beckmann et al., 2015; Rackham et al., 2012). All three RNase P subunits are identified by HL-1 cell interactome capture, indicating they each directly contact RNA. Remarkably, mutations in HSD17B10 cause progressive neurological abnormalities and cardiomyopathy in a manner that is unrelated to the protein's dehydrogenase activity (Deutschmann et al., 2014).

Twelve TCA cycle-related enzymes or enzyme subunits were identified as RBPs, covering most reaction steps (Figure 6A). Seven of these are further validated as RBPs by RBDmap data (depicted in Figure 7 and Figures S6D and S6E). We performed small-scale mRNA interactome capture experiments from HL-1 cells and probed western blots of material eluted from oligo(dT) beads with antibodies against six TCA cycle-related enzymes. This shows selective RNA-mediated purification of four of the six enzymes (Figure 6B; ACO2, CS, IDH2, OGDH). We also constructed a series of plasmids expressing enzymes C-terminally tagged with eGFP, transfected them into HeLa cells alongside positive (Pumilio-eGFP) and negative controls (eGFP alone, eGFP carrying an N-terminal mitochondrial localization signal),

and confirmed their expression (Figure S5D) and intracellular localization (Figure S5E).

Next, we immunopurified these fusion proteins from UV-crosslinked or control cells and subjected RNase-treated isolates to ^{32}P 5′ end labeling with polynucleotide kinase. This confirmed selective direct RNA association of fusion proteins in four cases (Figure 6C, left; ACO2, CS, IDH2, PDHA1). For ACO2, CS, IDH2, and MDH2, we also replicated these findings when performing pull-down and labeling from lysates of purified mitochondria (Figure 6C, right; Figure S5F). In summary, we obtained additional validation of RNA binding for ten TCA cycle-related enzymes by at least one method and two of them, IDH2 and ACO2, score positively in all four validation assays.

RNA Binding and Metabolic Enzyme Function

We used RBDmap data for 24 metabolic enzymes to explore the relationship between RNA, substrate, and cofactor binding, taking into account available information on tertiary and quaternary structure. Focusing on the TCA cycle, the monomeric enzyme ACO2 is particularly interesting as its cytoplasmic counterpart ACO1/IRP1 is well known for its dual enzyme/RBP functions (Muckenthaler et al., 2008). An RBDpep is situated on one flank of the iron-sulfur cluster-containing cleft of ACO2 (Figures 7A and 7A′). Comparison to the crystal structure of IRP1 bound to the ferritin IRE-RNA stem-loop (Walden et al., 2006) (Figure 7A′, right) suggests a similar mode of RNA binding to the active site cleft of ACO2, although, as the predicted Xpep also extends further, RNA contact with the outer surface of the enzyme is also plausible. The mitochondrial TCA cycle enzyme NAD$^+$-dependent IDH3 is a hetero-tetramer consisting of two α, one β, and one γ subunit. No mammalian structures have been reported; all subunits are similar in sequence yet carry out specialized functions. An RBDpep is found at the C terminus of the α subunit (IDH3A; Figure 7B), and structural modeling locates it to the periphery of the monomer, away from regions important for catalysis (Figure 7B′). The two NADP$^+$-utilizing IDH isoforms, cytosolic IDH1 and mitochondrial IDH2, each have R-f topology and form homodimers. Here, the Npeps overlap with the active site cleft, while the extended Xpeps reside just outside of the R-f on the protein surface (Figures S6D, S6D′, S6E, and S6E′).

DLD forms homodimers that serve as the E3 component of two large hetero-oligomeric assemblies, the pyruvate dehydrogenase complex, which links glycolysis to the TCA cycle, and the TCA cycle-integral oxoglutarate dehydrogenase complex. Here, the Xpep regions extend throughout the surface that binds
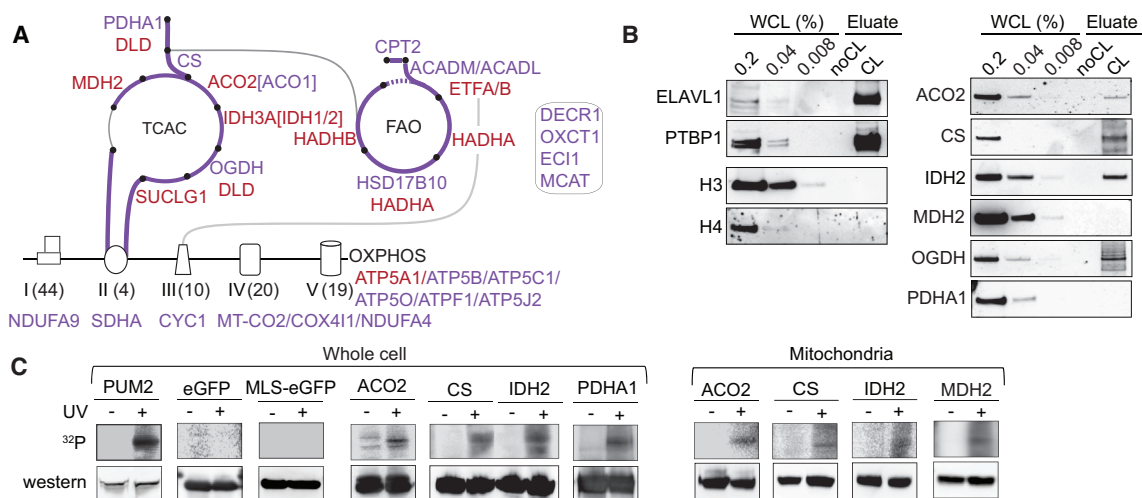
Figure 6. Validation of RNA Binding by Mitochondrial Enzymes

(A) Schematic of mitochondrial TCA cycle, FAO, and OXPHOS. Color scheme is as in Figure 4F. Number of known subunit variants for each OXPHOS complex is shown in brackets. NDUFA4 is considered as complex IV subunit (Balsa et al., 2012). Box to the right indicates FAO-associated enzymes.

(B) Small-scale mRNA interactome capture from HL-1 cells and western blots with antibodies against positive and negative controls (left; as in Figure 1C) as well as six endogenous TCA cycle-related enzymes (right; n = 1).

(C) Immunoprecipitation of eGFP-tagged proteins from UV-treated and control HeLa cells and ^{32}P 5′ end labeling of crosslinked RNA fragments. Samples were processed for storage phosphor imaging (top) and western blot with anti-GFP antibody (bottom). PUM2-eGFP (at lower dose) is shown as a positive control, while eGFP alone, with or without a mitochondrial localization signal, and mock purifications from non-crosslinked cells served as negative controls (n = 1–3). Immunoprecipitation was done from WCL (left) or from purified mitochondria (right). Controls for intracellular localization of fusion proteins and mitochondrial isolation are shown in Figure S5.

See also Figure S5.

FAD but also include sections on the protein surface (Figures 7C and 7C′). Succinyl-CoA ligase is a heterodimer formed by the substrate-binding subunit, SUCLG1, and SUCLG2, which binds GDP. RBDpeps tag both R-f of SUCLG1 with solvent-exposed Npep portions located away from the enzyme's active site (Figures 7D and 7D′). MDH2 functions as a homodimer and the two RBDpeps in the central and C-terminal regions lie outside the R-f on the surface of the dimer (Figures 7E and 7E′).

The two glycolysis enzymes PGK1 and LDHB continue an emerging theme. PGK1 (Figure 4H) possesses two R-f and functions as a monomer. The RBDpep is located on the outer edge of the substrate-binding N-terminal R-f of PGK1 with one extended Xpep adjacent to the active site and the other facing away from it on the outer surface, while ATP binds to the C-terminal R-f. LDHB (Figure 4I) and the aforementioned non-enzymatic ETF complex (Figure 3E) present similar cases. Altogether, we examined 24 metabolic enzymes (additional examples shown in Figures S6 and S7) and noted diverse spatial relationships between RBDmap peptides and enzyme active sites. While mutually exclusive RNA binding and catalytic function must be expected in a few cases, surprisingly, a common theme shared by most examples is the potential for concurrent RNA binding and enzyme activity, suggesting the possibility of allosteric or scaffolding functions for RNA.

DISCUSSION

We present here a comprehensive analysis of RNA-binding proteins in cardiomyocytes, constituting a rich resource of 1,148

cardiomyocyte RBPs and 568 regions of RNA contact within 368 of these RBPs. The data document and characterize the activity of many previously known RBPs in the cardiac context. For instance, just over half of the RBPs had prior RNA-related annotation and RBDmap identified RNA contact regions within recognized RBDs for many previously uncharacterized examples. Most interestingly, 393 of our RBPs were not seen in published interactomes. Among these will be some that remained undetected in past studies for technical reasons, but many were likely revealed here due to specific aspects of cardiomyocytic gene expression, metabolism, and function.

Over 200 of our RBPs have annotated roles in the cardiovascular system and/or are encoded by OMIM disease genes, and roughly half of these have no prior association with RNA biology. As expected, neurological disorders are prominent among the diseases linked to RBPs (Castello et al., 2013). Uniquely, almost half of the OMIM-RBPs identified here have links to metabolic or cardiovascular disorders. RBDmap identifies RNA contacts within 71 OMIM-RBPs, frequently overlapping with disease-causing mutations, and thus providing entry points into molecular exploration of disease relevance. The calcium channel SERCA2 is a case in point. RNA binding to its cytosolic domain may affect the function of SERCA2 in cardiac contractility and may thus represent a therapeutic target during heart failure. The RNA-binding region of SERCA2 further coincides with the location of mutations causing Darier's disease (Figure 3C).

Another feature of our data is the rich coverage of mitochondrial RNA biology. Around 190 proteins from mitochondria
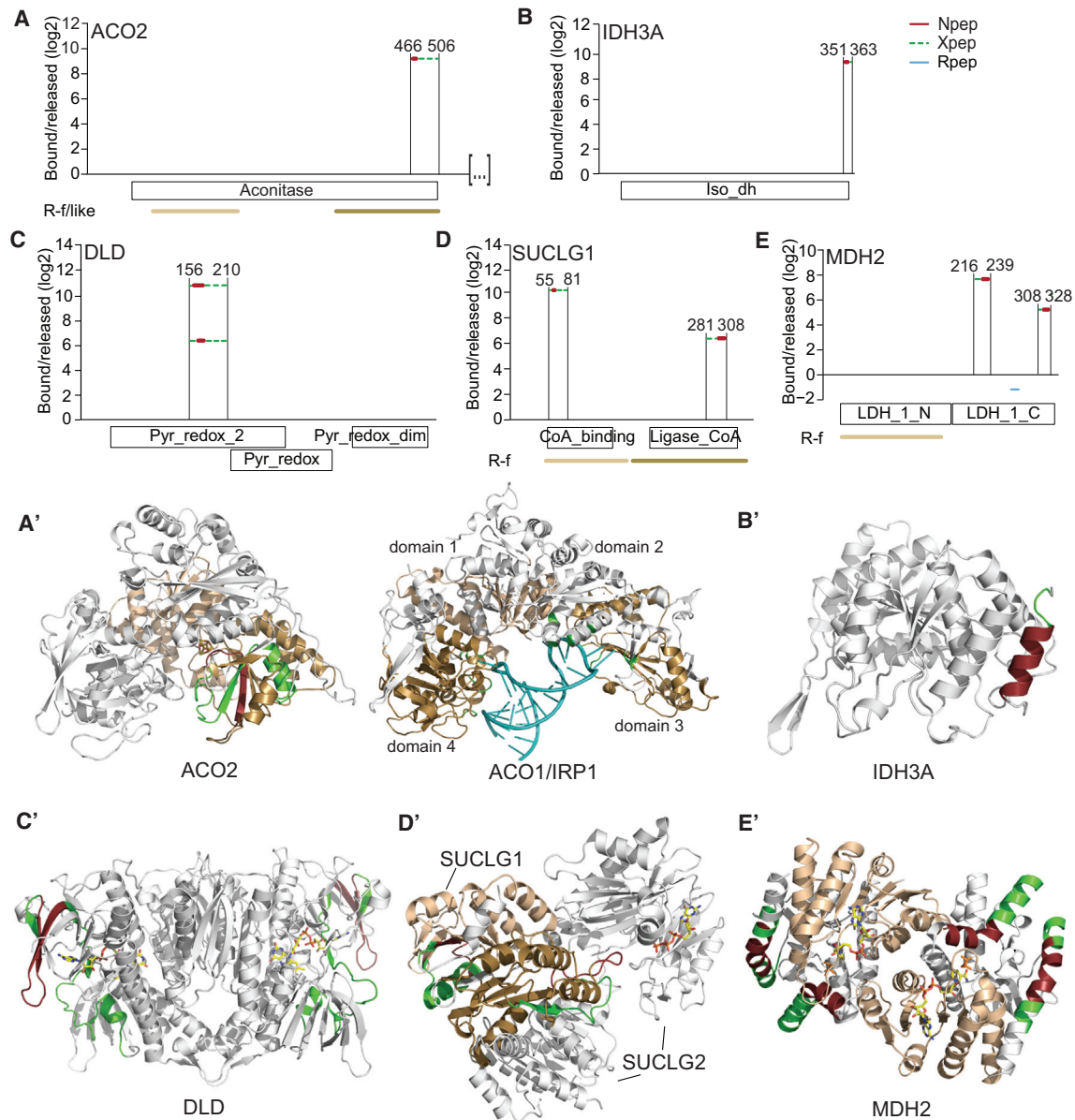
Figure 7. RNA-Binding Modalities among TCA Cycle Enzymes

(A–E) RBDmap data for ACO2 (amino acids 1–523; EC:4.2.1.3), IDH3A (EC:1.1.1.41), DLD (EC:1.8.1.4), SUCLG1 (EC:6.2.1.4, EC:6.2.1.5), and MDH2 (EC:1.1.1.37).

(A′–E′) RBDpeps were mapped to enzyme crystal or Phyre2-modeled structures.

(A′) ACO2 crystal structure with 4Fe-4S cluster (multicolor) (PDB: 6ACN) shown on left. IRP1/ACO1 co-crystal structure with IRE-RNA (teal) (PDB: 3SNP) shown for comparison on right; IRE contacts in IRP1 are depicted in green.

(B′) Phyre2-modeled structure of IDH3A.

(C′) Crystal structure of DLD dimer in complex with FAD (multicolor) (PDB: 1ZMC).

(D′) Crystal structure of SUCLG1-SUCLG2 heterodimer in complex with GTP (multicolor) (PDB: 2FP4).

(E′) Crystal structure of MDH2 dimer in complex with D-malate (orange) and NAD^+ (multicolor) (PDB: 2DFD).

See also Figures S6 and S7 and Tables S2 and S5.

were found to be active as RBPs in cardiomyocytes, and only roughly half of them had prior RNA-related annotation. This work independently confirms the link to RNA for the latter group, which includes many examples for which a clear role in the mitochondrial RNA life cycle has yet to be defined (Rackham et al.,

2012). The other half of the mtRBPs lacks prior RNA-related annotation, opening up rich prospects for discovery. This might particularly apply to the 49 mitochondrial metabolic enzymes we identified as RBPs, densely covering the energy-generating pathways of the TCA cycle, FAO, and OXPHOS. What could

be the function of enzyme-RNA binding? One possibility is that a subset of enzyme molecules, perhaps in response to metabolite levels or flux through the associated pathway, could moonlight as RNA regulators. This is not without precedent in mitochondria: the MRPP2 subunit of mitochondrial RNase P has an alter ego as an NAD$^+$-dependent short-chain fatty acid dehydrogenase (Rackham et al., 2012). It is tempting to speculate that ACO2, in analogy to its cytosolic counterpart ACO1/IRP1 (Muckenthaler et al., 2008), functions in post-transcriptional regulation of mitochondrial mRNA expression. Future work will need to identify RNA targets for ACO2 and the many other interesting leads discovered here to unveil the physiological relevance of their interactions with RNA. In some cases, this might even reveal roles of RBPs outside of their usual mitochondrial localization.

Overall, the 1,148 cardiomyocyte RBPs are less acidic and hydrophobic than the cellular proteome and are enriched in intrinsically disordered, low-complexity, and repetitive regions. They further display enrichment of RNA-related functional and domain annotation. This independently confirms similar observations made with the compositionally quite distinct HeLa mRNA interactome (Castello et al., 2012). The RBDmap approach extends these observations. Relative to the released protein fragments, RBDpeps are enriched for positively charged aromatic and small amino acids, as befits RNA interaction surfaces. The majority of them also lie within disordered protein regions, which retain a similar amino acid bias, indicating that disordered protein regions represent surprisingly common sites of RNA contact. Again, even though made on the basis of a largely distinct peptide set, these findings concur with parallel observations made by applying RBDmap to HeLa cells (Castello et al., 2016). RBDmap marks well-understood RNA-binding domains with high accuracy and implicates several globular protein domains not previously expected to contact RNA, such as the pro-isomerase domain found in PPIases. Protein domains of the Rossmann fold are common among the cardiomyocyte RBPs, prominently found in RNA helicases and the RNA-binding enzymes. RBDmap affirms the expected and relatively uniform mode of RNA binding to helicases, which mostly share the same R-f topology. By contrast, not all RNA-binding enzymes have R-f domains, and those that do are of more varied topology. Accordingly, RBDmap delineates a diverse range of RNA-binding modalities for the metabolic enzymes.

RNA binding to so many metabolic enzymes and other proteins with functions apparently unrelated to RNA might suggest novel roles of RNA in affecting protein function, rather than the reverse. In the case of enzymes, roles as competitive inhibitor, allosteric regulator, or as an assembly scaffold are conceivable (Castello et al., 2015). We have interpreted RBDmap data for multiple metabolic enzymes in the context of their known tertiary and quaternary structures, and, while this does not resemble formal proof, we have found that the most straightforward explanation for the data as a whole is that RNA binding and catalytic activity need not clash.

RNA binding often applies to multiple enzymes functioning in a given pathway. Assembly of a pathway metabolon with superior metabolic flux properties has been described for the TCA cycle (Vélot et al., 1997; Wu and Minteer, 2015), among other pathways. It is thus an exiting possibility that RNAs may provide as-

sembly scaffolds for metabolons, as suggested by the RNase-sensitivity of a complex of glycolytic enzymes (Mazurek et al., 1996). Such a role of RNA in metabolism would not be too dissimilar to scaffolding functions of noncoding RNAs in RNP aggregation, such as NEAT1 in paraspeckle assembly (Bond and Fox, 2009). Methods to biochemically isolate metabolons should be applied to search for putative RNA scaffolds in future work.

Altogether, we present here a comprehensive compendium of RNA-binding proteins active in cardiomyocytes and a survey of the regions they use to contact RNA. This work provides a fertile resource to study RNA-level regulation and its interfaces to other cellular processes in the context of mitochondrial function, cardiac (patho)physiology, and genetic disease.

EXPERIMENTAL PROCEDURES

A detailed version of the experimental procedures can be found in the Supplemental Information.

Cell Culture
HL-1 cardiomyocytes (a gift from W. Claycomb) were maintained as described (Claycomb et al., 1998). HeLa cells were purchased from ATCC and maintained by standard procedures.

mRNA Interactome Capture
Beating HL-1 cells were irradiated with UV light at 254 nm. Cells were lysed, and RNA-protein complexes were captured on oligo(dT)$_{25}$ magnetic beads, which were washed, eluted, and processed for mass spectrometry essentially as described (Castello et al., 2012).

RBDmap
Following mRNA interactome capture as detailed above, eluted RNA-protein complexes were digested with Lys-C followed by recapture on oligo(dT)$_{25}$ beads, separating a released fraction from RNA bound peptides, which were again eluted from the beads. Both released and RNA bound fractions were processed for mass spectrometry. RBDmap is described in Castello et al. (2016).

LC-MS/MS
An LTQ-Orbitrap Velos Pro mass spectrometer (Thermo Scientific) coupled to a nanoAcquity UPLC system (Waters) was used for detection of peptides in WCL, mRNA interactome, and RBDmap fractions.

Statistical Analysis and Interpretative Bioinformatic Analyses
Approaches to test for significance and for detecting ontology, pathway and disease association/enrichment, as well as protein sequence and other features are detailed in the Supplemental Information.

RNA-Binding Assays with eGFP-tagged RBPs
eGFP-RBP fusion plasmids were transfected into HeLa cells before irradiation with UV light at 254 nm. Cells or mitochondria were lysed, and RNA-fusion protein complexes were then captured on GFP-Trap beads and digested with RNase T1 before 5′ end labeling with γ-^{32}P-ATP by T4 PNK, anti-GFP western blot, and storage phosphor imaging.

Data Availability
The R scripts and source code used for data analyses can be found at: http://fischerlab.dkfz.de/cardiomyocyteInteractome/, and https://github.com/PreissLab/cardiomyocyteInteractome.

ACCESSION NUMBERS

The accession numbers for the mass spectrometry data reported in this paper are PRIDE: PXD002541 and PXD002543.

REFERENCES

Antonicka, H., and Shoubridge, E.A. (2015). Mitochondrial RNA granules are centers for posttranscriptional RNA processing and ribosome biogenesis. Cell Rep. 10, 920–932.

Balsa, E., Marco, R., Perales-Clemente, E., Szklarczyk, R., Calvo, E., Landázuri, M.O., and Enríquez, J.A. (2012). NDUFA4 is a subunit of complex IV of the mammalian electron transport chain. Cell Metab. 16, 378–386.

Baltz, A.G., Munschauer, M., Schwanhäusser, B., Vasile, A., Murakawa, Y., Schueler, M., Youngs, N., Penfold-Brown, D., Drew, K., Milek, M., et al. (2012). The mRNA-bound proteome and its global occupancy profile on protein-coding transcripts. Mol. Cell 46, 674–690.

Beckmann, B.M., Horos, R., Fischer, B., Castello, A., Eichelbaum, K., Alleaume, A.M., Schwarzl, T., Curk, T., Foehr, S., Huber, W., et al. (2015). The RNA-binding proteomes from yeast to man harbour conserved enigmRBPs. Nat. Commun. 6, 10127.

Bond, C.S., and Fox, A.H. (2009). Paraspeckles: nuclear bodies built on long noncoding RNA. J. Cell Biol. 186, 637–644.

Brauch, K.M., Karst, M.L., Herron, K.J., de Andrade, M., Pellikka, P.A., Rodeheffer, R.J., Michels, V.V., and Olson, T.M. (2009). Mutations in ribonucleic acid binding protein gene cause familial dilated cardiomyopathy. J. Am. Coll. Cardiol. 54, 930–941.

Busch, A., and Hertel, K.J. (2012). Evolution of SR protein and hnRNP splicing regulatory factors. Wiley Interdiscip. Rev. RNA 3, 1–12.

Caetano-Anollés, G., Kim, H.S., and Mittenthal, J.E. (2007). The origin of modern metabolic networks inferred from phylogenomic analysis of protein architecture. Proc. Natl. Acad. Sci. USA 104, 9358–9363.

Castello, A., Fischer, B., Eichelbaum, K., Horos, R., Beckmann, B.M., Strein, C., Davey, N.E., Humphreys, D.T., Preiss, T., Steinmetz, L.M., et al. (2012). Insights into RNA biology from an atlas of mammalian mRNA-binding proteins. Cell 149, 1393–1406.

Castello, A., Fischer, B., Hentze, M.W., and Preiss, T. (2013). RNA-binding proteins in Mendelian disease. Trends Genet. 29, 318–327.

Castello, A., Hentze, M.W., and Preiss, T. (2015). Metabolic enzymes enjoying new partnerships as RNA-binding proteins. Trends Endocrinol. Metab. 26, 746–757.

Castello, A., Fischer, B., Frese, C.K., Horos, R., Alleaume, A.-M., Föhr, S., Curk, T., Krijgsveld, J., and Hentze, M.W. (2016). Comprehensive identification of RNA-binding domains in human cells. Mol Cell 63. http://dx.doi.org/10.1016/j.molcel.2016.06.029.

Chen, C.Y., and Shyu, A.B. (2014). Emerging mechanisms of mRNP remodeling regulation. Wiley Interdiscip. Rev. RNA 5, 713–722.

Cieśla, J. (2006). Metabolic enzymes that bind RNA: yet another level of cellular regulatory network? Acta Biochim. Pol. 53, 11–32.

Claycomb, W.C., Lanson, N.A., Jr., Stallworth, B.S., Egeland, D.B., Delcarpio, J.B., Bahinski, A., and Izzo, N.J., Jr. (1998). HL-1 cells: a cardiac muscle cell line that contracts and retains phenotypic characteristics of the adult cardiomyocyte. Proc. Natl. Acad. Sci. USA 95, 2979–2984.

Copley, S.D. (2012). Moonlighting is mainstream: paradigm adjustment required. BioEssays 34, 578–588.

Dango, S., Mosammaparast, N., Sowa, M.E., Xiong, L.J., Wu, F., Park, K., Rubin, M., Gygi, S., Harper, J.W., and Shi, Y. (2011). DNA unwinding by ASCC3 helicase is coupled to ALKBH3-dependent DNA alkylation repair and cancer cell proliferation. Mol. Cell 44, 373–384.

Daubner, G.M., Cléry, A., Jayne, S., Stevenin, J., and Allain, F.H. (2012). A syn-anti conformational difference allows SRSF2 to recognize guanines and cytosines equally well. EMBO J. 31, 162–174.

Deutschmann, A.J., Amberger, A., Zavadil, C., Steinbeisser, H., Mayr, J.A., Feichtinger, R.G., Oerum, S., Yue, W.W., and Zschocke, J. (2014). Mutation or knock-down of 17β-hydroxysteroid dehydrogenase type 10 cause loss of MRPP1 and impaired processing of mitochondrial heavy strand transcripts. Hum. Mol. Genet. 23, 3618–3628.

Eimre, M., Paju, K., Pelloux, S., Beraud, N., Roosimaa, M., Kadaja, L., Gruno, M., Peet, N., Orlova, E., Remmelkoor, R., et al. (2008). Distinct organization of energy metabolism in HL-1 cardiac cell line and cardiomyocytes. Biochim. Biophys. Acta 1777, 514–524.

Fairman-Williams, M.E., Guenther, U.P., and Jankowsky, E. (2010). SF1 and SF2 helicases: family matters. Curr. Opin. Struct. Biol. 20, 313–324.

Filipovska, A., and Rackham, O. (2013). Pentatricopeptide repeats: modular blocks for building RNA-binding proteins. RNA Biol. 10, 1426–1432.

Fiorini, F., Boudvillain, M., and Le Hir, H. (2013). Tight intramolecular regulation of the human Upf1 helicase by its N- and C-terminal domains. Nucleic Acids Res. 41, 2404–2415.

Gorski, P.A., Ceholski, D.K., and Hajjar, R.J. (2015). Altered myocardial calcium cycling and energetics in heart failure–a rational approach for disease treatment. Cell Metab. 21, 183–194.

Guo, W., Schafer, S., Greaser, M.L., Radke, M.H., Liss, M., Govindarajan, T., Maatz, H., Schulz, H., Li, S., Parrish, A.M., et al. (2012). RBM20, a gene for hereditary cardiomyopathy, regulates titin splicing. Nat. Med. 18, 766–773.

Hall, M.P., Nagel, R.J., Fagg, W.S., Shiue, L., Cline, M.S., Perriman, R.J., Donohue, J.P., and Ares, M., Jr. (2013). Quaking and PTB control overlapping splicing regulatory networks during muscle cell differentiation. RNA 19, 627–638.

Hentze, M.W. (1994). Enzymes as RNA-binding proteins: a role for (di)nucleotide-binding domains? Trends Biochem. Sci. 19, 101–103.

Hentze, M.W., and Preiss, T. (2010). The REM phase of gene regulation. Trends Biochem. Sci. 35, 423–426.

Jaffrey, S.R. (2014). An expanding universe of mRNA modifications. Nat. Struct. Mol. Biol. 21, 945–946.

Jourdain, A.A., Koppen, M., Wydro, M., Rodley, C.D., Lightowlers, R.N., Chrzanowska-Lightowlers, Z.M., and Martinou, J.C. (2013). GRSF1 regulates RNA processing in mitochondrial RNA granules. Cell Metab. *17*, 399–410.

Kato, M., Han, T.W., Xie, S., Shi, K., Du, X., Wu, L.C., Mirzaei, H., Goldsmith, E.J., Longgood, J., Pei, J., et al. (2012). Cell-free formation of RNA granules: low complexity sequence domains form dynamic fibers within hydrogels. Cell *149*, 753–767.

Keene, J.D. (2007). RNA regulons: coordination of post-transcriptional events. Nat. Rev. Genet. *8*, 533–543.

Kim, H.J., Kim, N.C., Wang, Y.D., Scarborough, E.A., Moore, J., Diaz, Z., MacLea, K.S., Freibaum, B., Li, S., Molliex, A., et al. (2013). Mutations in prion-like domains in hnRNPA2B1 and hnRNPA1 cause multisystem proteinopathy and ALS. Nature *495*, 467–473.

King, O.D., Gitler, A.D., and Shorter, J. (2012). The tip of the iceberg: RNA-binding proteins with prion-like domains in neurodegenerative disease. Brain Res. *1462*, 61–80.

König, J., Zarnack, K., Luscombe, N.M., and Ule, J. (2012). Protein-RNA interactions: new genomic technologies and perspectives. Nat. Rev. Genet. *13*, 77–83.

Kramer, K., Sachsenberg, T., Beckmann, B.M., Qamar, S., Boon, K.L., Hentze, M.W., Kohlbacher, O., and Urlaub, H. (2014). Photo-cross-linking and high-resolution mass spectrometry for assignment of RNA-binding sites in RNA-binding proteins. Nat. Methods *11*, 1064–1070.

Kwon, S.C., Yi, H., Eichelbaum, K., Föhr, S., Fischer, B., You, K.T., Castello, A., Krijgsveld, J., Hentze, M.W., and Kim, V.N. (2013). The RNA-binding protein repertoire of embryonic stem cells. Nat. Struct. Mol. Biol. *20*, 1122–1130.

Lightowlers, R.N., and Chrzanowska-Lightowlers, Z.M. (2013). Human pentatricopeptide proteins: only a few and what do they do? RNA Biol. *10*, 1433–1438.

Loedige, I., Jakob, L., Treiber, T., Ray, D., Stotz, M., Treiber, N., Hennig, J., Cook, K.B., Morris, Q., Hughes, T.R., et al. (2015). The crystal structure of the NHL domain in complex with RNA reveals the molecular basis of Drosophila brain-tumor-mediated gene regulation. Cell Rep. *13*, 1206–1220.

Mahadevan, K., Zhang, H., Akef, A., Cui, X.A., Gueroussov, S., Cenik, C., Roth, F.P., and Palazzo, A.F. (2013). RanBP2/Nup358 potentiates the translation of a subset of mRNAs encoding secretory proteins. PLoS Biol. *11*, e1001545.

Matia-González, A.M., Laing, E.E., and Gerber, A.P. (2015). Conserved mRNA-binding proteomes in eukaryotic organisms. Nat. Struct. Mol. Biol. *22*, 1027–1033.

Mazurek, S., Hugo, F., Failing, K., and Eigenbrodt, E. (1996). Studies on associations of glycolytic and glutaminolytic enzymes in MCF-7 cells: role of P36. J. Cell. Physiol. *167*, 238–250.

Méthot, N., Song, M.S., and Sonenberg, N. (1996). A region rich in aspartic acid, arginine, tyrosine, and glycine (DRYG) mediates eukaryotic initiation factor 4B (eIF4B) self-association and interaction with eIF3. Mol. Cell. Biol. *16*, 5328–5334.

Mitchell, S.F., Jain, S., She, M., and Parker, R. (2013). Global analysis of yeast mRNPs. Nat. Struct. Mol. Biol. *20*, 127–133.

Mondal, T., Rasmussen, M., Pandey, G.K., Isaksson, A., and Kanduri, C. (2010). Characterization of the RNA content of chromatin. Genome Res. *20*, 899–907.

Muckenthaler, M.U., Galy, B., and Hentze, M.W. (2008). Systemic iron homeostasis and the iron-responsive element/iron-regulatory protein (IRE/IRP) regulatory network. Annu. Rev. Nutr. *28*, 197–213.

Ostareck, D.H., Ostareck-Lederer, A., Wilm, M., Thiele, B.J., Mann, M., and Hentze, M.W. (1997). mRNA silencing in erythroid differentiation: hnRNP K and hnRNP E1 regulate 15-lipoxygenase translation from the 3′ end. Cell *89*, 597–606.

Perrucci, G.L., Gowran, A., Zanobini, M., Capogrossi, M.C., Pompilio, G., and Nigro, P. (2015). Peptidyl-prolyl isomerases: a full cast of critical actors in cardiovascular diseases. Cardiovasc. Res. *106*, 353–364.

Rackham, O., Mercer, T.R., and Filipovska, A. (2012). The human mitochondrial transcriptome and the RNA-binding proteins that regulate its expression. Wiley Interdiscip. Rev. RNA *3*, 675–695.

Rosca, M.G., Tandler, B., and Hoppel, C.L. (2013). Mitochondria in cardiac hypertrophy and heart failure. J. Mol. Cell. Cardiol. *55*, 31–41.

Rossmann, M.G., Moras, D., and Olsen, K.W. (1974). Chemical and biological evolution of nucleotide-binding protein. Nature *250*, 194–199.

Schiene-Fischer, C. (2015). Multidomain Peptidyl Prolyl cis/trans Isomerases. Biochim. Biophys. Acta *1850*, 2005–2016.

Schiff, M., Froissart, R., Olsen, R.K., Acquaviva, C., and Vianey-Saban, C. (2006). Electron transfer flavoprotein deficiency: functional and molecular aspects. Mol. Genet. Metab. *88*, 153–158.

Shen, H., and Green, M.R. (2006). RS domains contact splicing signals and promote splicing by a common mechanism in yeast through humans. Genes Dev. *20*, 1755–1765.

Sibbritt, T., Patel, H.R., and Preiss, T. (2013). Mapping and significance of the mRNA methylome. Wiley Interdiscip. Rev. RNA *4*, 397–422.

Sillitoe, I., Lewis, T.E., Cuff, A., Das, S., Ashford, P., Dawson, N.L., Furnham, N., Laskowski, R.A., Lee, D., Lees, J.G., et al. (2015). CATH: comprehensive structural and functional annotations for genome sequences. Nucleic Acids Res. *43*, D376–D381.

Singh, G., Pratt, G., Yeo, G.W., and Moore, M.J. (2015). The clothes make the mRNA: past and present trends in mRNP fashion. Annu. Rev. Biochem. *84*, 325–354.

Vélot, C., Mixon, M.B., Teige, M., and Srere, P.A. (1997). Model of a quinary structure between Krebs TCA cycle enzymes: a model for the metabolon. Biochemistry *36*, 14271–14276.

Walden, W.E., Selezneva, A.I., Dupuy, J., Volbeda, A., Fontecilla-Camps, J.C., Theil, E.C., and Volz, K. (2006). Structure of dual function iron regulatory protein 1 complexed with ferritin IRE-RNA. Science *314*, 1903–1908.

Wu, F., and Minteer, S. (2015). Krebs cycle metabolon: structural evidence of substrate channeling revealed by cross-linking and mass spectrometry. Angew. Chem. Int. Ed. Engl. *54*, 1851–1854.

Zheng, L., Jiang, H., Mei, Q., and Chen, B. (2015). Identification of two novel Darier disease-associated mutations in the ATP2A2 gene. Mol. Med. Rep. *12*, 1845–1849.